Stochastic magnetic field driven charge transport and zonal flow during magnetic reconnection[a]

W. X. Ding,[1,2,b] D. L. Brower,[1,2] D. Craig,[2,3] B. E. Chapman,[2] D. Ennis,[2,4] G. Fiksel,[2,4] S. Gangadhara,[2,4] D. J. Den Hartog,[2,4] V. V. Mirnov,[2,4] S. C. Prager,[2,4] J. S. Sarff,[2,4] V. Svidzinski,[4] P. W. Terry,[2,4] and T. Yates[1]

[1]*Department of Physics and Astronomy, University of California at Los Angeles, Los Angeles, California 90095, USA*
[2]*Center for Magnetic Self-Organization in Astrophysical and Laboratory Plasmas, University of Wisconsin–Madison, Madison, Wisconsin 53706, USA*
[3]*Department of Physics, Wheaton College, Wheaton, Illinois 60187, USA*
[4]*Physics Department, University of Wisconsin-Madison, Madison, Wisconsin 53706, USA*

Magnetic fluctuation-induced charge transport, resulting from particle transport that is not intrinsically ambipolar, has been measured in the high-temperature interior of a reversed-field pinch plasma. It is found that global resistive tearing modes and their nonlinear interactions lead to significant charge transport, equivalent to the perpendicular Maxwell stress, in the vicinity of the resonant surface for the dominant core resonant mode during magnetic reconnection. Finite charge transport can result in a zonal flow associated with locally strong radial electric field and electric field shear. In the presence of stochastic magnetic field, radial electric field is expected to be balanced by radial electron pressure gradient. Direct measurement of local density gradient is consistent with the formation of radial electric field and the zonal flow. © *2008 American Institute of Physics*. [DOI: 10.1063/1.2837047]

I. INTRODUCTION

Magnetic fluctuations have been long recognized as a likely cause of anomalous particle, momentum and energy transport in various magnetic confinement devices.[1–5] In particular, particle transport due to stochastic magnetic fields is not intrinsically ambipolar since electrons stream rapidly along field lines. These stochastic magnetic fields can be driven by global tearing instabilities that often underlie the sawtooth oscillation and degrade overall confinement.[1,3] Conversely, externally imposed magnetic perturbations (as in ergodic divertors) can act to mitigate edge-localized modes (ELMs) by locally enhancing edge transport without loss of core plasma confinement[6] and have generated new interest in understanding the role played by stochastic magnetic fields in transport.

Magnetic fluctuation-induced particle transport has been studied for many years (see Ref. 4, and references therein) but all previous measurements were made by probes and consequently limited to the cooler edge region of hot plasmas. In the edge, it was found that particle losses induced by magnetic field fluctuations were ambipolar.[7–9] More recent measurements, with probes that are inserted deeper into the plasma,[10] indicate that the difference between electron and ion losses due to magnetic fluctuations could be nonzero. Unlike electrostatic fluctuation-induced particle transport, magnetic fluctuation-induced transport is not intrinsically ambipolar. Any nonintrinsic ambipolar transport (i.e., finite charge transport) across the equilibrium magnetic field will change the radial electric field (E_r) which adjusts to reflect the imbalance between electron and ion fluxes. These fields can then act to generate a zonal flow.

A radial electric field can in principle arise from multiple plasma processes, e.g., classical and neoclassical diffusion, ion orbit loss, pressure gradient or turbulence-driven Reynolds stresses.[11] Theoretically, a nonintrinsic ambipolar flux driven by one mechanism can exist but must be balanced by an opposing nonintrinsic ambipolar flux driven by another mechanism to maintain plasma quasineutrality.[12] Furthermore, it has been shown that the charge flux is not pointwise zero for a localized normal mode and ambipolarity can still be realized on a spatial average.[13] This implies a local radial electric field structure may exist as a consequence of finite charge transport. The combined effects of radial electric field and stochastic magnetic field play an important role in the Madison Symmetric Torus (MST) reversed-field pinch (RFP) and may also be relevant to other toroidal confinement devices.

In this paper, we experimentally explore the case where magnetic field lines become stochastic during the crash phase of a sawtooth oscillation corresponding to a magnetic reconnection event in the RFP configuration. Magnetic fluctuation-induced charge flux related to the dominant core resonant mode is measured directly using a nonperturbing, high-speed, laser-based Faraday rotation diagnostic. Measurements show that the radial charge flux from magnetic fluctuations alone is nonzero ($\sim 1\%$ of the total radial particle flux) and localized to the mode-resonant surface. This charge flux by itself would lead to a huge radial electric field. However, the effect is largely offset by the ion polarization drift across magnetic surfaces. The net result, *calculated* from the measured magnetic fluctuation-induced flux

(including the inferred polarization drift, viscous damping, and diamagnetic drift), is a charge separation that produces a potential well with large radial electric field and radial electric field shear, leading to a zonal flow at the resonant surface. In the presence of stochastic magnetic field, the local radial electric field is expected to be balanced by radial electron pressure gradient since electrons can freely stream along stochastic field lines. The measured local density gradient, $-\partial n_e / \partial r$, transiently increases near the resonant surface during a magnetic reconnection event, consistent with the predicted radial electric field structure. Furthermore, this magnetic fluctuation-induced charge flux is experimentally found to depend on nonlinear mode-mode coupling to alter the phase relation between current density and magnetic fluctuations.

The paper is organized as follows: In Sec. II, we introduce the concepts and general equations for stochastic magnetic field driven particle (and charge) transport, radial electric field, and zonal flow. Experimental measurement of charge transport and electron density gradient are presented in Sec. III. In Sec. IV, we discuss experimental results and their implications. A summary of the paper and conclusions are provided in Sec. V.

II. TRANSPORT IN STOCHASTIC MAGNETIC FIELDS

A. Particle (charge) transport due to stochastic magnetic field

Stochastic magnetic field induced particle transport can be described as the projection of the parallel particle flux along the radial direction in a toroidal device,[4,5]

$$\Gamma_{r,\alpha} = \langle \Gamma_{\|,\alpha} \vec{b} \cdot \vec{e}_r \rangle, \tag{1}$$

where $\Gamma_{\|,\alpha}$ is parallel particle flux for species α (electron or ion), $\vec{b} = \vec{B}/B$ is a unit vector of magnetic field, $\vec{e}_r$ is a radial unit vector, and $\langle \cdots \rangle$ denotes a magnetic surface average. Both the parallel flux and magnetic field can be decomposed into mean and fluctuating components, i.e., $\Gamma_{\|,\alpha} = \Gamma_{\|0,\alpha} + \delta\Gamma_{\|,\alpha}$, $\vec{b} = \vec{b}_0 + \delta\vec{b}$. Thus, the magnetic fluctuation-induced radial particle flux can be written as

$$\Gamma_{r,\alpha} = \frac{\langle \delta j_{\|,\alpha} \delta b_r \rangle}{q_\alpha B}, \tag{2}$$

where $\delta j_{\|,\alpha} = q_\alpha \delta\Gamma_{\|,\alpha}$ is the species current density fluctuation parallel to the equilibrium magnetic field $\vec{B}$, and δb_r is the radial magnetic field fluctuation while mean radial magnetic field is zero. The difference between electron flux and ion flux is defined as charge flux (Γ_q),

$$\Gamma_q = \Gamma_{r,i} - \Gamma_{r,e} = \frac{\langle \delta j_{\|} \delta b_r \rangle}{eB}, \tag{3}$$

where $\delta j_{\|}$ is the net parallel current density fluctuation. Since $\Gamma_q \ll \Gamma_{r,i}, \Gamma_{r,e}$, it is not feasible to accurately determine the

charge flux by measuring parallel electron and ion fluctuating fluxes separately and taking their difference. However, charge flux can be directly obtained by measuring magnetic field fluctuations only since parallel current fluctuations can be related to magnetic fluctuations via Ampere's law.

It is useful to express Eq. (3) in a form most suitable for experimental determination. For simplicity, we derive an expression in x, y, z coordinates where the equilibrium magnetic field is $\vec{B} = B_y \vec{e}_y + B_z \vec{e}_z$ and the magnetic perturbation is $\delta\vec{b} \sim \delta\vec{b}(x)\exp(ik_y y + ik_z z)$. The magnetic surface average $\langle \cdots \rangle$ is defined as $\iint dy dz$ and $\langle i\delta b_j \delta b_j \rangle = 0$ ($j = x, y, z$) due to $\pi/2$ phase difference between $i\delta b_j$ and δb_j. Using Ampere's law, $\nabla \times \delta\vec{b} = \mu_0 \delta\vec{J}$, we obtain

$$\langle \delta j_{\|} \delta b_x \rangle = \langle \delta j_y \delta b_x \rangle \frac{B_y}{B} + \langle \delta j_z \delta b_x \rangle \frac{B_z}{B}$$
$$= -\frac{1}{\mu_0} \left\langle \delta b_x \frac{\partial}{\partial x} \delta b_z \right\rangle \frac{B_y}{B} + \frac{1}{\mu_0} \left\langle \delta b_x \frac{\partial}{\partial x} \delta b_y \right\rangle \frac{B_z}{B}. \tag{4}$$

From Gauss's law, $\nabla \cdot \delta\vec{b} = 0$, we substitute $\delta b_z = -k_y / k_z \delta b_y + i/k_z \partial/\partial x \delta b_x$ into Eq. (4) and generate the expression

$$\langle \delta j_{\|} \delta b_x \rangle = \frac{1}{\mu_0 k_z} \left(k_y \frac{B_y}{B} + k_z \frac{B_z}{B} \right) \left\langle \delta b_x \frac{\partial}{\partial x} \delta b_y \right\rangle$$
$$= \frac{1}{\mu_0 B k_z} (\vec{k} \cdot \vec{B}) \left\langle \delta b_x \frac{\partial}{\partial x} \delta b_y \right\rangle. \tag{5}$$

By noting that $\langle \delta j_z \delta b_x \rangle = 1/\mu_0 \langle \partial \delta b_y / \partial x \delta b_x \rangle$, we can write the charge flux as

$$\frac{\langle \delta j_{\|} \delta b_x \rangle}{eB} = \frac{1}{eB^2 k_z} (\vec{k} \cdot \vec{B}) \langle \delta j_z \delta b_x \rangle. \tag{6}$$

By now switching to cylindrical coordinates ($x \to r, y \to \theta, z \to \phi$) which is appropriate for MST plasmas, the flux-surface-averaged quantity can be rewritten approximately as

$$\Gamma_q = \frac{\langle \delta j_{\|} \delta b_r \rangle}{eB} \cong \frac{R}{neB^2} (\vec{k} \cdot \vec{B}) \langle \delta j_\phi \delta b_r \rangle, \tag{7}$$

where $\vec{k} \cdot \vec{B} = n/RB_\phi + m/rB_\theta$, and ϕ, θ, and r are the toroidal, poloidal, and radial directions, respectively. An additional term arising in cylindrical coordinates, $\sim \langle \delta b_r \delta b_\theta \rangle / r^2$, is not included in Eq. (7) as it is found to be small in the vicinity of the resonant surface, $|(r - r_s)/r_s| \ll 1$, where r_s is the resonant surface location.[14] From Eqs. (6) and (7), it becomes clear that the charge flux is zero at the mode resonant surface since $k_{\|} = 0$ and changes the sign across the resonant surface due to the magnetic shear. Thus, charge flux can be experimentally obtained by measuring all quantities in Eq. (7).

B. Transport and perpendicular flow

For low-frequency electromagnetic and electrostatic fluctuations ($\omega \ll \omega_{ci}$), where ω_{ci} is ion gyrofrequency, the total radial flux of ions (Γ_i^T) and electrons (Γ_e^T) can be written in the form,[13,15]

$$\Gamma_i^T = n_i V_i^r = \frac{nM}{eB_0}\frac{\partial \langle V_\perp^i\rangle}{\partial t} - \frac{\vec{F}_{\perp,i}^c \times \vec{B}_0}{eB_0^2} + \frac{\langle \delta j_{\parallel,i}\delta b_r\rangle}{eB_0} + \frac{\langle \tilde{n}_i \tilde{E}_\perp\rangle}{B_0},$$

(8a)

$$\Gamma_e^T = n_e V_e^r = -\frac{n_e m}{eB_0}\frac{\partial \langle V_\perp^e\rangle}{\partial t} + \frac{\vec{F}_{\perp,e}^c \times \vec{B}_0}{eB_0^2} - \frac{\langle \delta j_{\parallel,e}\delta b_r\rangle}{eB_0}$$

$$+ \frac{\langle \tilde{n}_e \tilde{E}_\perp\rangle}{B_0}.$$

(8b)

These two equations are equivalent to the ion and electron perpendicular momentum equations, respectively.

The first term on the right-hand side is ion (electron) drift due to ion (electron) inertial force. The second term is the ion (electron) $\vec{F}_{\perp,i}^c \times \vec{B}_0$ (or $\vec{F}_{\perp,e}^c \times \vec{B}_0$) drift, where $\vec{F}_{\perp,i}^c(\vec{F}_{\perp,e}^c)$ is the classical collision force density acting on ions (electrons) within the magnetic surface perpendicular to B_0. The third term is the magnetic fluctuation-induced ion (electron) particle flux [see Eq. (2)] and the last term is the electrostatic fluctuation-induced convective particle flux, where $\tilde{E}_\perp$ corresponds to perpendicular electric field fluctuations.[4] Global quasineutrality requires $\Gamma_i^T - \Gamma_e^T \approx 0$. Thus, by evaluating the difference between Eqs. (8a) and (8b), we find

$$\rho\frac{\partial}{\partial t}\langle V_\perp^i\rangle - \mu_\perp \nabla^2 \langle V_\perp^i\rangle = \langle \delta j_\parallel \delta b_r\rangle = eB_0 \Gamma_q.$$

(9)

Since the electron inertial and collision terms are negligible compared to ion terms, we only keep the ion collision term $F_{\perp,i}^c = -\mu_\perp \nabla^2 V_\perp^i$, where $v^* = \mu_\perp/\rho(\sim 0.3 Z_{eff} nkT_i/\omega_{ci}^2 \tau_i)$, and ρ, Z_{eff}, τ_i are mass density, effective ionic charge, and collision time, respectively.[16]

According to Eq. (9), perpendicular flow is driven by magnetic fluctuation-induced charge flux and dissipated by classical perpendicular viscosity. Charge flux is essentially equivalent to the perpendicular Lorentz force or Maxwell stress. The fluctuation-induced perpendicular Lorentz force is $\langle \delta \vec{j} \times \delta \vec{b}\rangle_\perp = 1/\mu_0 \langle \nabla \cdot \delta \vec{b}\delta \vec{b}\rangle_\perp$, where $\langle \delta \vec{b}\delta \vec{b}\rangle$ is referred to as the Maxwell stress tensor.[17] Within the magnetic surface, this force induces radial charge flux

$$\frac{\langle \delta\vec{j} \times \delta\vec{b}\rangle_\perp \times \vec{B}_0}{B_0^2} = \frac{\langle \delta j_\parallel \delta b_r - \delta j_r \delta b_\parallel\rangle}{B_0} \approx \frac{\langle \delta j_\parallel \delta b_r\rangle}{B_0}$$

(10)

since in the vicinity of resonant surface $(k_\parallel \approx 0)$ $\delta j_\parallel \gg \delta j_r \approx 0$ and $\delta b_r \gg \delta b_\parallel$ hold for the tearing instabilities.

Let us compare Eq. (9) to standard zonal flow equation in a tokamak,[17]

$$\rho\frac{\partial}{\partial t}\langle V_\theta\rangle + \eta\langle V_\theta\rangle = -\frac{\partial}{\partial r}\left[\langle \delta v_r \delta v_\theta\rangle - \frac{1}{\mu_0}\langle \delta b_r \delta b_\theta\rangle\right], \quad (11)$$

where η is a magnetic pumping coefficient. It is worth mentioning that electrostatic fluctuation-induced charge transport does not enter Eqs. (9) explicitly since its transport is ambipolar. However, charge flux can result from the perpendicular

ion Reynolds force $F_\perp^{Re} = nM\langle \delta v_r 1/r \partial/\partial r r \delta v_\perp\rangle$ driven by electrostatic turbulence. This force is believed to generate zonal flows in tokamaks.[17] It is easy to recognize from Eq. (9) that the perpendicular flow is driven by charge flux (Maxwell stress, $\langle \delta b_r \delta b_\theta\rangle$ term) and dissipated by classical viscous force while Reynolds stress ($\langle \delta v_r \delta v_\theta\rangle$ term) is neglected.

C. Radial electric field and density gradient

Localized radial electric field is expected to be accompanied by a local density gradient according to radial force balance for each species,

$$V_\perp^i = -\frac{E_r}{B} + \left(\frac{T_i \nabla n_i}{n_i eB} + \frac{\nabla T_i}{eB}\right),$$

(12a)

$$V_\perp^e = -\frac{E_r}{B} - \left(\frac{T_e \nabla n_e}{n_e eB} + \frac{\nabla T_e}{eB}\right).$$

(12b)

A more direct relation between E_r and ∇n_e is obtained by Harvey who treats electron dynamics arising from the stochastic magnetic field.[18] Global quasineutrality requires $E_r = -T_e/e\frac{\partial}{\partial r}[\ln(n_e T_e^{1/2})]$, indicating that electrons nearly satisfy adiabatic force balance along chaotic magnetic field lines.[19] If we ignore ∇T_e and assume $T_e \approx T_i$, we find $E_r = -T_e/e\langle \frac{1}{n_e}\partial n_e/\partial r\rangle$. Comparing Eqs. (12a) and (12b), this would correspond to $V_\perp^i \approx -2E_r/B$ and $V_\perp^e \approx 0$. This heuristic discussion leads to the radial electric field diffusion equation, with a form similar to that of Eq. (9) for perpendicular flow,

$$\varepsilon_0 \varepsilon_\perp \frac{\partial\langle E_r\rangle}{\partial t} - \frac{\mu_\perp}{B_0^2}\nabla^2\langle E_r\rangle = -\frac{\langle \delta j_\parallel \delta b_r\rangle}{2B_0},$$

(13)

where $\varepsilon_\perp$ is a perpendicular dielectric constant.

Equations (9) and (13) clearly indicate that the zonal flow and radial electric field [or electron density gradient from Eqs. (12)] can be driven by nonzero charge flux in plasmas. This interrelation provides motivation to measure the charge flux[20] and search for a localized density gradient associated with radial electric field formation.

III. EXPERIMENTAL RESULTS

Measurements reported herein were carried out on the MST (Refs. 21 and 22) device whose major radius $R_o = 1.5$ m, minor radius $a = 0.52$ m, discharge current 350–400 kA, line-averaged electron density $\bar{n}_e \sim 1 \times 10^{19}$ m^{-3}, electron temperature $T_e \sim T_i \sim (300-350)$ eV, and $Z_{eff} = 2-6$. Equilibrium and fluctuating magnetic fields are measured by a fast (time response up to 1 μs) Faraday rotation diagnostic where 11 chords (separation ~ 8 cm) probe the plasma cross section vertically.[14] MST discharges display a sawtooth cycle in many parameters and measured quantities are ensemble (flux-surface) averaged over these reproducible sawtooth events. All fluctuation measurements refer to the dominant core-resonant resistive-tearing mode
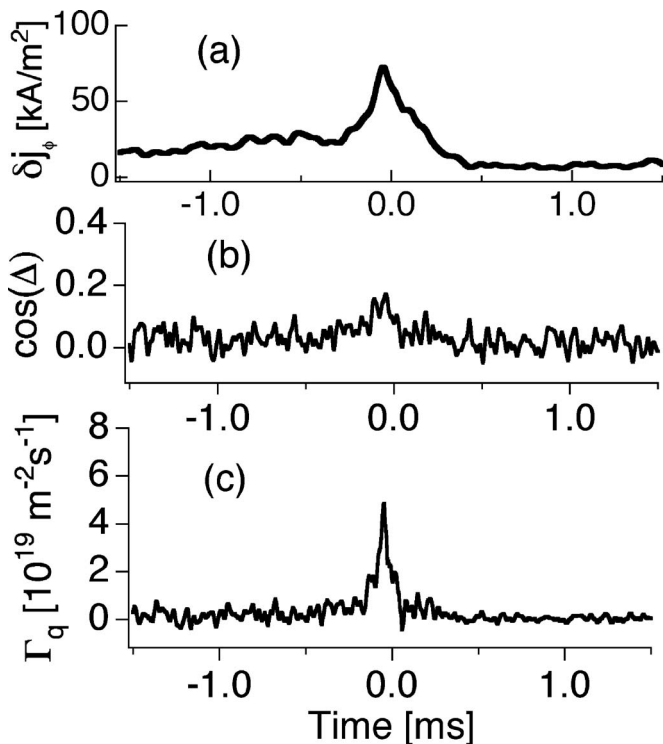
FIG. 1. (a) Current fluctuations; (b) phase between current and magnetic field fluctuation for $m/n=1/6$ mode; (c) the charge flux. The $t=0$ denotes the sawtooth crash.
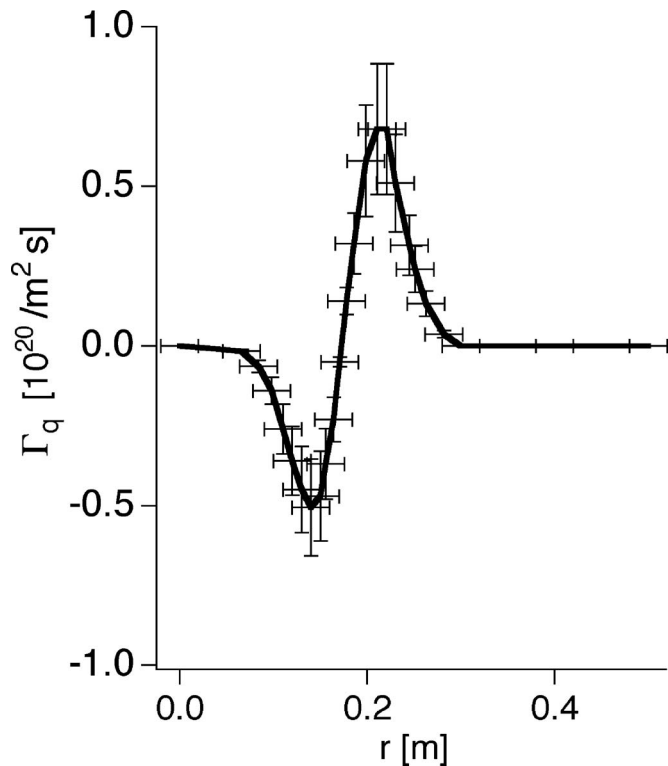

FIG. 2. Magnetic fluctuation-induced charge flux (equivalent to the perpendicular component of Maxwell stress) spatial distribution. Flux changes sign across the resonant surface at $r=0.17$ m.

($m/n=1/6$ where m and n are poloidal and toroidal mode number) with laboratory frame frequency $\sim 15-20$ kHz whose resonant surface is located at $r/a=0.35$.

A. Charge flux measurement

The charge flux spatial profile is determined by measuring the radial dependence of all quantities in Eq. (7). The radial derivative of δb_θ is directly obtained by measuring current density fluctuations (δj_ϕ) using a novel polarimetry analysis technique which invokes Ampere's law to evaluate the current density between adjacent chords directly.[14,23] The phase information between δj_ϕ and δb_r is evaluated by ensemble averaging. In MST, toroidal rotation of $m/n=1/6$ magnetic modes transfers their spatial structure in the plasma frame into a temporal evolution in the laboratory frame. Since the magnetic modes are global, for convenience we correlate δj_ϕ to a specific helical magnetic mode obtained from spatial Fourier decomposition of measurements from 64 wall-mounted magnetic coils. After averaging over an ensemble of similar events, we can directly determine the phase between δj_ϕ and $\delta b_\theta(a)$ for the specified mode. Since the radial magnetic perturbation is expected to have a constant phase at all radii for tearing modes (which has been verified by probe measurements in lower temperature plasmas), we can infer the phase between δj_ϕ and δb_r where the phase difference between δb_r and $\delta b_\theta(a)$ is $\pi/2$ at the conducting wall. Toroidal current density fluctuations slowly increase during the linear phase of the sawtooth cycle and surge at the crash as shown in Fig. 1(a). The phase (Δ) between toroidal current density and radial magnetic field fluctuations is

nearly $\pi/2$ away from the sawtooth crash, making the cosine of phase near zero as shown in Fig. 1(b). This implies the magnetic fluctuation-induced particle transport is approximately ambipolar. However, when approaching the crash, the phase deviates from $\pi/2$ and fluctuation amplitudes increase thereby generating significant magnetic fluctuation-induced charge flux. The charge flux spatial maxima over a sawtooth event is seen in Fig. 1(c), and shows a peak of $\sim 4 \times 10^{19}$ m^{-2} s^{-1} at the crash. This is less than 1% of the measured total radial particle flux.[24]

The radial magnetic and current density fluctuation profiles have been measured for the dominant core resonant ($m/n=1/6$) mode just prior to the sawtooth crash.[14,23] By combining this result with equilibrium magnetic field profile,[24] we are able to obtain the spatial profile of charge flux (or perpendicular Maxwell stress) [Eq. (7)] at a sawtooth crash as seen in Fig. 2. Charge flux is zero at the resonant surface because $\vec{k} \cdot \vec{B}=0$. However, on either side of the resonant surface the charge flux is nonzero and changes sign due to magnetic shear (i.e., $\vec{k} \cdot \vec{B}$ changes sign across the resonant surface).

B. Origin of charge flux

The existence of nonvanishing charge flux in MST plasmas appears to require nonlinear interactions between multiple modes. Experimentally, observed changes in fluctuation amplitude [Fig. 1(a)] and phase [Fig. 1(b)] during a sawtooth crash act to drive the charge flux. In MST, resonant $m=1$ magnetic modes dominate the core magnetic fluctuation
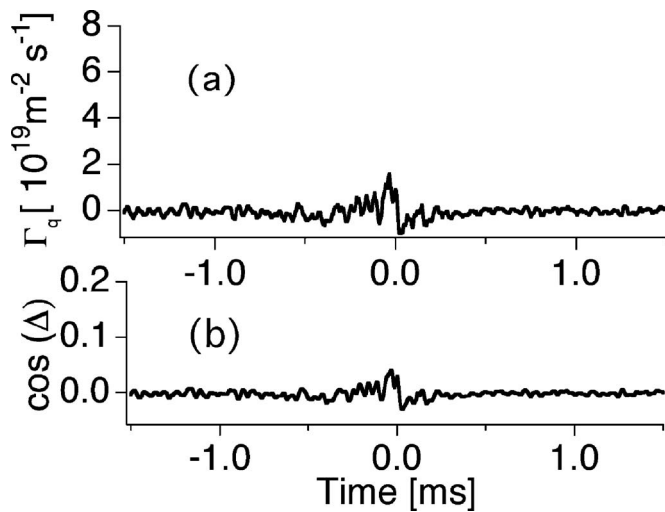
FIG. 3. (a) Magnetic induced charge flux dynamics over the sawtooth for plasmas where the $m=0$ mode is removed; (b) phase between current fluctuations and radial magnetic fluctuations where the $m=0$ mode is removed.
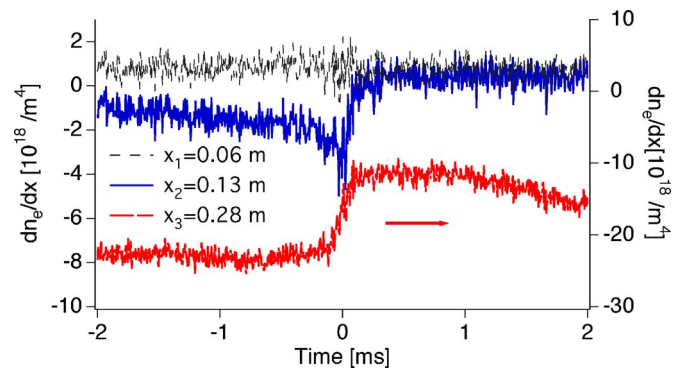

FIG. 4. (Color online) Electron density gradient dynamics over the sawtooth crash for three impact parameters. Near the resonant surface ($x_2=0.13$ m) the electron density gradient increases at the sawtooth crash, which is associated with the local increase of the radial electric field driven by charge flux.

wave number spectrum. In addition to the core resonant modes, $m=0$ modes (which are observed as a burst at the crash) are resonant at the reversal surface ($r/a \sim 0.8$) where the toroidal magnetic field goes to zero (near the plasma edge). Both the $m=1$ and $m=0$ tearing modes have a global nature so that nonlinear mode coupling is common. Any three-wave interaction has to satisfy the sum rule $m_1 \pm m_2 = m_3$ and $n_1 \pm n_2 = n_3$. Coupling of two adjacent $m=1$ modes via interaction with an $m=0$ mode has been shown to be very important in both experiments and MHD computation.[25–27]

A typical strong three wave interaction observed in MST plasmas is that between the $(m=1, n=6)$, $(1,7)$ and $(0,1)$ modes. By suppressing one of the interacting modes, we can reduce the nonlinear mode coupling. In order to identify the role played by nonlinear coupling in the charge flux during the sawtooth crash, we compare standard RFP plasmas with those where the reversal surface has been removed (i.e., nonreversed plasmas). For nonreversed plasmas, the $m=1$ mode amplitude $[\delta b_\theta(a)]$ during the sawtooth cycle remains comparable to the reversed case. However, the $m=0$ mode amplitude is significantly reduced since its resonant surface is removed. As shown in Fig. 3(a), the charge flux for these plasmas is reduced up to fivefold compared to standard RFP plasmas seen earlier in Fig. 1(c). This occurs primarily because the phase difference between δj_ϕ and δb_r for the $(1,6)$ mode is also altered, deviating only slightly from $\pi/2$, as shown in Fig. 3(b). This suggests the phase change between δj_ϕ and δb_r for the $(1,6)$ mode is related to nonlinear mode-mode coupling.

C. Electron density gradient measurement

Local electron density gradient measurements have recently been made possible using a newly developed differential interferometer technique.[28] The differential interferometer measures the difference of line-integrated electron density $\partial \bar{n}_e / \partial x$ between two very closely spaced chords (effective separation $\Delta x \sim 1$ mm), where $\bar{n}_e(x) = 1/L \int n_e(r) dz$.

Evolution of ensemble-averaged line-averaged electron density gradient $\langle \partial \bar{n}_e / \partial x \rangle$ over sawtooth crash is shown in Fig. 4. The electron density gradient shows no change just before sawtooth crash for central chord (impact parameter $x_1 = 0.06$ m). Near the resonant surface ($x_2 = 0.13$ m), line-averaged electron density gradient ($-\langle \partial \bar{n}_e / \partial x \rangle$) transiently increases by a factor of 2 immediately prior to a sawtooth crash ($-0.3 < t < 0$ ms). The line-averaged electron density gradient does not increase away from the resonant surface ($x_3 = 0.28$ m) for the same time period. This suggests the electron density gradient locally increases as opposed to global density change. Locally, the sign of $-\langle \partial \bar{n}_e / \partial x \rangle$ (for $x_2 = 0.13$ m) is *positive* (radially pointing outward). Quantitative measurement of diamagnetic drift requires a precise local density measurement in addition to accurate density gradient measurement. In principle, the local density gradient can be obtained by inversion of the line-averaged measurements. However, for the chords close to the magnetic axis, one can estimate the local density gradient directly. From the relation $\partial \bar{n}_e(x)/\partial x = (1/L) \int [\partial n_e(r)/\partial r](x/r) dz = (1/L) \times \int [\partial n_e(r)/\partial r] \cos \theta dz$, we have $\partial \bar{n}_e(x)/\partial x \approx \partial \bar{n}_e/\partial r \times \int \cos \theta dz = \partial \bar{n}_e/\partial r \times (0.30 \sim 0.50)$. Spatial resolution is significantly improved due to the geometrical weighting factor $\cos(\theta)$. Local density at sawtooth crash is measured to be $(0.7-0.8) \times 10^{19}$ m^{-3}, therefore the estimated equivalent electric field $(E_r = -T_e/e \langle \frac{1}{n_e} \partial n_e / \partial r \rangle)$ due to density gradient is $500-800$ V/m at sawtooth crash.

IV. DISCUSSIONS

The experimentally determined nonvanishing charge flux indicates that magnetic fluctuation-induced particle transport is not intrinsically ambipolar and the radial electric field will be altered. It is observed that magnetic fluctuation-induced charge flux is about $(4.0 \times 10^{19}/m^2 s)$. In the core of MST plasmas, ion velocity fluctuations are measured to be the order of $0.5-1$ km/s. This leads to a maximum charge flux of $\sim 0.6 \times 10^{19}/m^2$ s if velocity fluctuations are 100% correlated and have spatial scale ~ 5 cm. Thus, the maximum ion velocity fluctuation-induced charge transport is much less than magnetic fluctuation-induced charge flux. Therefore ion

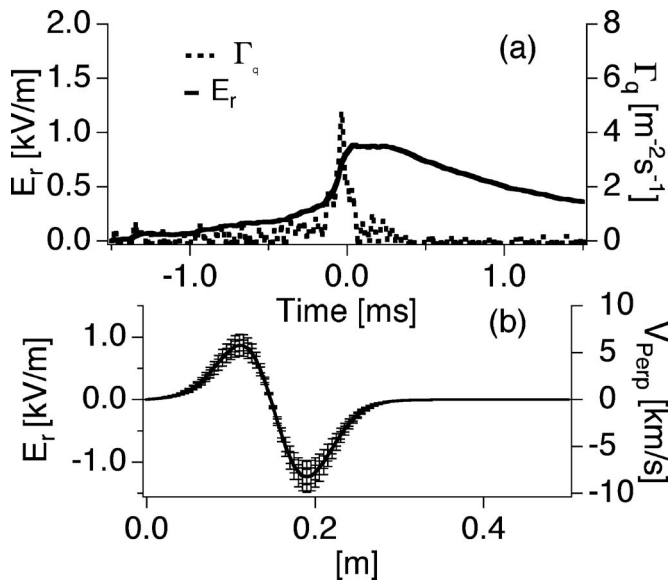FIG. 5. (a) Radial electric field dynamics and charge flux over a sawtooth cycle. $t<0$ corresponds to times before the sawtooth crash. (b) Radial electric field profile and $E \times B$ flow profile after the sawtooth crash ($t=0.25$ ms). The variation of B with minor radius is ignored here.
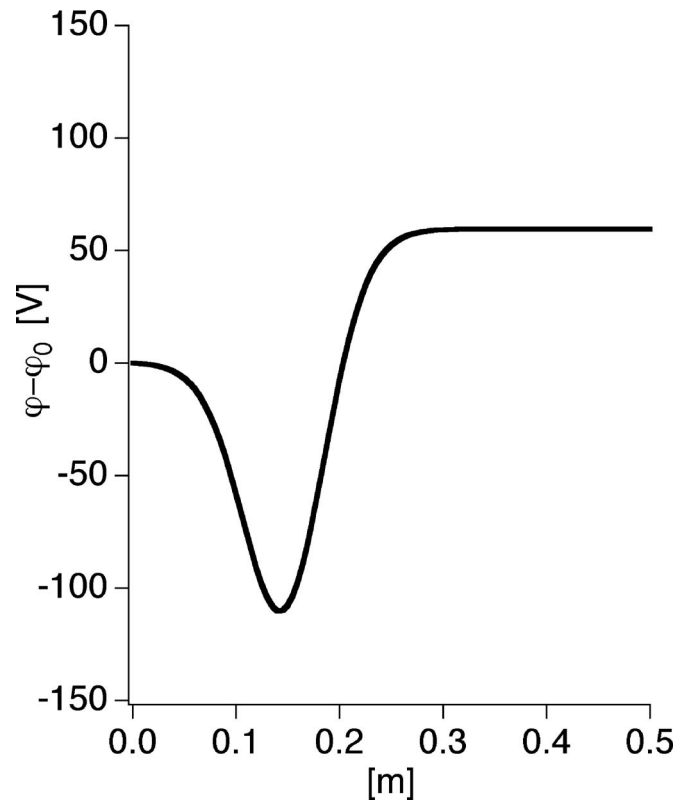

FIG. 6. Calculated potential spatial profile at the sawtooth crash ($t=0.25$ ms). It shows the potential well near the resonant surface.

Reynolds stress induced charge flux[29] can be neglected in Eq. (9). Other effects such as neoclassical diffusion and charge exchange are expected to be small in the core of MST plasmas.

Consequently, the evolution of radial electric field can be governed by Eq. (13) which is a diffusion equation for radial electric field. The typical radial electric field diffusion time is of the order ($\sim a^2/\nu^* \sim 500$ ms) where $Z_{eff}=6$ is used for estimation. This dissipation time is usually much longer than a MST discharge (~ 100 ms). However, the dissipation may not be negligible if a small-scale radial electric field develops as is implied near the mode resonant surface. To provide an estimate of radial electric field, numerical integration of Eq. (13) is performed using boundary conditions $E_r(0)=E_r(a)=0$ along with the measured charge flux at the resonant surface. Temporal dynamics of the computed radial electrical field are shown in Fig. 5(a). The radial electric field is small and slowly increasing prior to a sawtooth crash due to a small magnetic fluctuation-induced charge flux at this time. A maximum is reached after a surge of charge flux at the sawtooth crash while the polarization drift goes to zero ($dE_r/dt=0$) when the charge flux is balanced by electric field diffusion. Since the charge flux diminishes after the crash, the radial electric field decays on a longer time scale due to viscous damping. It should be noted that the radial electric field is dissipated within a few ms [$\sim(\delta l)^2/\nu^*$] due to development of radial electric field having local shear with scale ($\delta l \sim 5$ cm) comparable to magnetic island width.

As shown in Fig. 5(b), the saturated radial field spatial profile (at $t=0.25$ ms) changes sign across the resonant surface in a fashion similar to charge flux [see Fig. 2(b)]. The radial electric field points toward the resonant surface on either side, indicating that a local potential well is created as shown in Fig. 6. The potential perturbation appears as a superposition on the equilibrium potential (φ_0). A maximum

radial electric field of 1 kV/m is reached just after sawtooth crash. The inferred radial electric field from charge flux is consistent with the estimated electric field (0.5–0.8 kV/m) by using electron radial force balance in Sec. III C, and at $r \lesssim r_s$ has a positive sign, the same as that for the electron diamagnetic field $-T_e \langle \frac{1}{n_e} \partial n_e / \partial r \rangle$. Although the inferred radial electric field from charge flux has a qualitative agreement with the measured electron density gradient change before sawtooth crash, it is observed that density gradient relaxes within a few hundred microsecond (see Fig. 4), much faster than the dissipation of radial electric field ~ 1 ms (modeled in the figure but not measured). The quantitative comparison between electron density gradient and radial electric field structure requires a radial electric field measurement which is expected in the future from the heavy ion beam probe on the MST.

Perpendicular flow dynamics are the same as that of the radial electric field as shown in Fig. 5(a) since the momentum equation [Eq. (9)] has the same form as the radial electric field equation [Eq. (13)]. The corresponding zonal flow spatial profile is shown in Fig. 5(b). Zero-mean-frequency flow driven by charge flux near the mode resonant surface has an $m=n=0$ zonal field structure since the ensemble averaged charge flux has an $m=n=0$ nature. This flow changes sign across the tearing mode resonant surface thereby imparting no net momentum on spatial average. An important result here is that even small magnetic fluctuation-induced charge flux is sufficient to generate a large zonal flow structure.

V. CONCLUSION

In conclusion, resistive tearing mode driven, magnetic fluctuation-induced particle transport has been experimentally measured in the core of a high-temperature plasma. The resulting charge flux dominates in the vicinity of the mode resonant surface and reverses sign across the resonant surface. Modeling indicates the measured charge flux, including shielding from the ion polarization drift and viscous damping, can result in the buildup of a significant radial electric field and electric field shear thereby generating a potential well. The flow pattern associated with this fluctuation-induced radial electric field has an $m=n=0$ zonal flow structure and can be dissipated on a slower timescale by classic collisions. Local measurement of electron density gradient is qualitatively consistent with the radial electric field formation, which implies that zonal flow also consists of diamagnetic components.[30] Furthermore, we find that three wave coupling plays an important role in charge flux by changing the phase between current density and radial magnetic field fluctuations. Future work will focus on direct measurement of the electric field and flow implied by the measured charge flux.

ACKNOWLEDGMENTS

[1] A. B. Rechester and M. N. Rosenbluth, Phys. Rev. Lett. **40**, 38 (1978).
[2] T. H. Stix, Phys. Rev. Lett. **18**, 833 (1973).
[3] J. Wesson, *Tokamaks* (Oxford University Press, New York, 1997), p. 189.
[4] P. C. Liewer, Nucl. Fusion **25**, 543 (1985).
[5] S. C. Prager, Plasma Phys. Controlled Fusion **32**, 903 (1990).
[6] K. H. Finken, S. S. Abdullaev, M. W. Jakubowski, M. F. de Bock, S. Bozhenkov, C. Bush, M. von Hellerman, R. Jaspers, Y. Kikuchi, A. Kraemer-Flecken, M. Lehnen, D. Schega, O. Schmitz, K. H. Spatschek, B. Unterberg, A. Wingen, R. C. Wolf, O. Zimmermann, and the TEXTOR team, Phys. Rev. Lett. **98**, 065001 (2007); T. E. Evans, R. A. Moyer, P. R. Thomas, J. G. Watkins, T. H. Osborne, J. A. Boedo, E. J. Doyle, M. E. Fenstermacher, K. H. Finken, R. J. Groebner, M. Groth, J. H. Harris, R. J. La Haye, C. J. Lasnier, S. Masuzaki, N. Ohyabu, D. G. Rhode, H. Reimerdes, D. L. Rudakov, M. J. Schaffer, G. Wang, and L. Zeng, Phys. Rev. Lett. **92**, 235001 (2004).
[7] M. R. Stoneking, S. A. Hokin, S. C. Prager, G. Fiskel, H. Ji, and D. J. Den Hartog, Phys. Rev. Lett. **73**, 549 (1994).
[8] T. D. Rempel, A. F. Almagri, S. Assadi *et al.*, Phys. Fluids B **4**, 2136 (1992).
[9] W. Shen, R. N. Dexter, and S. C. Prager, Phys. Rev. Lett. **68**, 1319 (1992).
[10] N. A. Crocker, Ph.D. dissertation, University of Wisconsin–Madison, 2001.
[11] K. Itoh and S. Itoh, Plasma Phys. Controlled Fusion **38**, 1 (1996); P. H. Diamond and Y.-B. Kim, Phys. Fluids A **3**, 1626 (1991); K. Itoh, S.-I. Ithoh, P. H. Diamond, T. S. Hahm, A. Fujisawa, G. R. Tynan, M. Yagi, and Y. Nagashima, Phys. Plasmas **13**, 05502 (2006); W. M. Solomon and M. G. Shats, Phys. Rev. Lett. **87**, 195003 (2001).
[12] T. E. Stringer, Nucl. Fusion **32**, 1421 (1992).
[13] R. E. Waltz, Phys. Fluids **25**, 1269 (1982).
[14] W. X. Ding, D. L. Brower, B. H. Deng, D. Craig, S. C. Prager, and V. Svidzinski, Rev. Sci. Instrum. **75**, 3387 (2004).
[15] S. Inoue, T. Tange, K. Itoh, and T. Tuda, Nucl. Fusion **19**, 1252 (1979).
[16] P. Helander and D. J. Sigmar, *Collisional Transport in Magnetized Plasma* (Cambridge University Press, New York, 2002), p. 90.
[17] P. W. Terry, Rev. Mod. Phys. **72**, 109 (2000).
[18] R. W. Harvey, M. G. McCoy, J. Y. Hsu, and A. A. Mirin, Phys. Rev. Lett. **47**, 102 (1981).
[19] J. M. Finn, P. N. Guzdar, and A. A. Chernikov, Phys. Fluids B **B4**, 1152 (1992).
[20] W. X. Ding, D. L. Brower, D. Craig, B. H. Deng, S. C. Prager, J. S. John, and V. Svidzinski, Phys. Rev. Lett. **99**, 055004 (2007).
[21] R. N. Dexter, D. W. Kerst, T. W. Lovell, S. C. Prager, and J. C. Sprott, Fusion Technol. **19**, 131 (1991).
[22] H. A. B. Bodin, Nucl. Fusion **30**, 1717 (1990).
[23] W. X. Ding, D. L. Brower, S. D. Terry, D. Craig, S. C. Prager, J. S. John, and J. C. Wright, Phys. Rev. Lett. **90**, 035002 (2003).
[24] S. D. Terry, D. L. Brower, W. X. Ding *et al.*, Phys. Plasmas **11**, 1079 (2004); N. E. Lanier, D. Craig, J. K. Anderson, T. M. Biewer, B. E. Chapman, D. J. Den Hartog, C. B. Forest, S. C. Prager, D. L. Brower, and Y. Jiang, *ibid.* **8**, 3402 (2001).
[25] A. K. Hansen, A. F. Almagri, D. Craig, D. J. Den Hartog, C. C. Hegna, S. C. Prager, and J. S. Sarff, Phys. Rev. Lett. **85**, 3408 (2000); S. Assadi, S. C. Prager, and K. L. Sidikman, *ibid.* **69**, 281 (1992).
[26] R. G. Watt and R. A. Nebel, Phys. Fluids **26**, 1168 (1983).
[27] T. Bolzonella and D. Terranova, Plasma Phys. Controlled Fusion **44**, 2569 (2002).
[28] W. X. Ding, D. L. Brower, B. H. Deng, and T. Yates, Rev. Sci. Instrum. **77**, 10F105 (2006).
[29] P. H. Diamond, Y.-M. Liang, B. A. Carreras, and P. W. Terry, Phys. Rev. Lett. **72**, 2565 (1994).
[30] R. E. Waltz, M. E. Austin, K. H. Burrell, and J. Candy, Phys. Plasmas **13**, 052301 (2006).